Design and Control of IPMSM Sensorless Drive for Mechanical Rotor Position Detection Capability

Yong-Cheol Kwon, and Seung-Ki Sul
School of Electrical & Computer Engineering
Seoul National University
Seoul, Korea
dydcjfe@eepel.snu.ac.kr, sulsk@plaza.snu.ac.kr

Noor Aamir Baloch, Sohji Murakami, and Shinya Morimoto
Energy Conversion Technology Group
YASKAWA ELECTRIC CORPORATION
12-1 Otemachi, Kokurakita-ku, Kitakyushu 803-8530, JAPAN
baloch@yaskawa.co.jp, smurakam@yaskawa.co.jp,
sinya@yaskawa.co.jp

***Abstract*—In this paper, a design and control method of Interior Permanent Magnet Synchronous Machines (IPMSMs), which is controlled in position sensorless mode based on high frequency signal injection, for absolute position detection and control capability has been addressed. Although conventional motor designs with symmetric structure work well in sensorless speed and torque control modes, their actual mechanical rotor position is unidentifiable since their inductance profile is repeated for every electrical revolution. In order to realize the mechanical rotor position detection capability, from a given template 6-pole/9-slot IPMSM with symmetric structure, an IPMSM design with asymmetric winding and asymmetric rotor geometry is proposed and constructed as a prototype. Based on the proposed design, the mechanical rotor position can be identified at the cost of slight degradation of basic motor characteristics such as torque ripples, harmonics in back EMF, and etc. The overall performances of the proposed IPMSM have been evaluated by rigorous FEM and experimental test.**

NOMENCLATURE

PP	number of pole-pairs.
θ_{rm}	mechanical rotor position.
θ_r	electrical rotor position, $PP \cdot \theta_{rm}$.
$\hat{\theta}_{rm}$	estimated value of θ_{rm}.
$\hat{\theta}_r$	estimated value of θ_r.
λ_f	back-EMF constant.
R_s	winding resistance.
L_{ds}, L_{qs}	d-q components of stator self-inductance.

I. INTRODUCTION

Nowadays, Interior Permanent Magnet Synchronous Machines (IPMSMs) are widely used in many industrial applications thanks to its higher torque density, higher efficiency, and flux weakening capability. In vector-controlled IPMSM drives which guarantee instantaneous torque control, one of the most fundamental information for the control is the rotor position. And, position sensors such as encoders and resolvers are normally used to extract the rotor position. However, the position sensors have brought about many concerns such as increased volume and cost of drive system, EMI issues, extra connector and wires, and reliability issues associated with sensor itself.

In order to escape from the problems of the position sensors, position-sensorless drive, simply sensorless drive, has been highlighted by many researchers [1]-[3]. For sensorless drive at standstill and low speed, in IPMSM sensorless drive, saliency based methods [2]-[3] are normally used. Spatial variation of inductance of IPMSM is clearly determined by the rotor position. By injecting high frequency voltage signal to the motor terminals and analyzing its resultant current behavior, the rotor position information can be extracted through simple signal processing of the measured current.

In conventional sensorless drives, the estimated rotor position is electrical rotor position, not mechanical rotor position. The electrical rotor position is enough for most AC motor drive applications since only the electrical rotor position is needed for the instantaneous torque control in rotor reference frame. However, for absolute position control applications such as robots and machine tools, actual mechanical rotor position should be identified and controlled. In these applications, regardless of the sensorless control capability of IPMSM, up to now, the additional absolute position sensor such as absolute encoder and resolver has been installed to identify the actual rotor position.

This paper proposes a design and control of IPMSM for sensorless drive, which has the capability of mechanical rotor position detection. Based on a template 6-pole/9-slot IPMSM with symmetric winding and symmetric rotor geometry, a modified motor design with asymmetric

978-1-4799-0336-8/13/$31.00 ©2013 IEEE

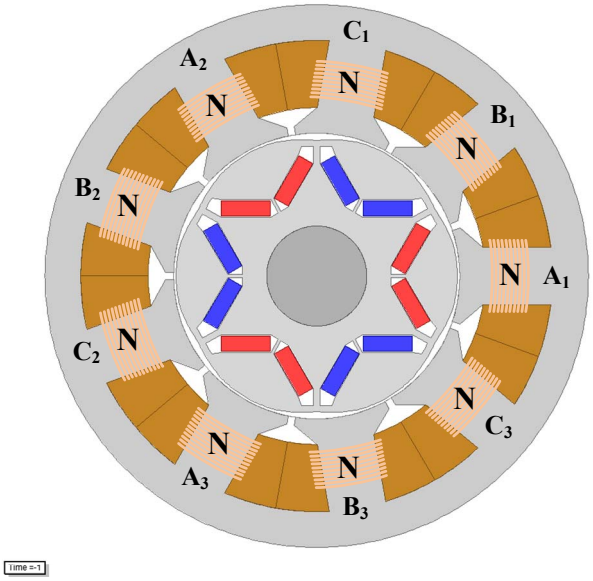

Figure 1. Cross-sectional diagram of template motor.

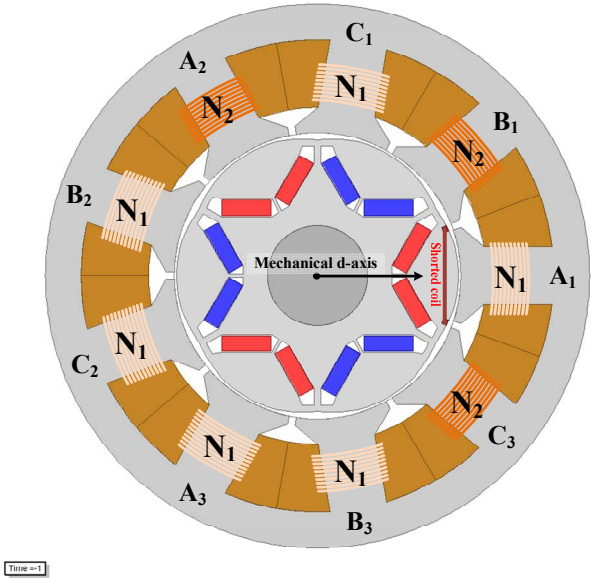

Figure 2. Motor design with rotor coil and non-uniform winding.

winding and asymmetric rotor shape is proposed. The basic performance of the proposed motor design has been evaluated through Finite Element Method (FEM), and the motor has been constructed as a prototype. Based on the devised motor design, an algorithm for detecting the mechanical rotor position detection is also developed. Finally, the mechanical rotor position control capability of the proposed IPMSM design is experimentally verified.

II. Motor Design for Mechanical Rotor Position Detection

In normal AC machines, the stator winding and the rotor shape are designed to be symmetric for every pole-pair. Then all electrical characteristics are repeated for *PP* times as the rotor rotates for mechanically one revolution. For example, inductance profiles with θ_{rm}=-110°, θ_{rm}=10°, and θ_{rm}=130° are all identical in normal 6-pole motors. And, if the θ_r is identified as 30°, θ_{rm} cannot be differentiated between -110° and 10°, and 130°. With asymmetric winding motors such as 8-pole/9-slot motors, the inductance profile also overlap 4 times for a single mechanical rotation of the rotor because rotor itself is normally designed to be symmetric. This is the reason why it is impossible to identify the mechanical rotor position of conventional motors under sensorless drive.

Fig. 1 shows a 6-pole/9-slot IPMSM design provided as a template design. As shown in Fig. 1, twelve permanent magnets are buried inside the rotor in V-shape. In the stator winding, 3 coils with N (40) turn are series connected at each phase, and 3 phase windings are linked by Y connection. The template motor specifications are given in Table 1. Like other symmetric AC machines, θ_{rm} of the prototype motor cannot be identified by sensorless drive due to its symmetric structure. The goal of this study is making the mechanical rotor position detection capability for the template motor by modifying its design, while minimizing the degradation of basic performance of the template motor.

TABLE I. Specifications of Template Motor

Rated speed	3000 r/min
Rated output power	300 W
Rated current	2.85 A_{rms}
Core material	Silicon steel
Permanent magnet material	NdFeB
Number of poles	6 poles
Stator winding	3-coil series, 3-phase star, concentrated winding
R_s	0.49 Ω
λ_f	0.065 V·s
L_{ds}	6.9 mH
L_{qs}	10.6 mH

A. Possible Combinantions of Stator and Rotor Designs

As aforementioned, it is impossible to extract θ_{rm} using symmetric machines. To achieve the mechanical position detection capability, both stator and rotor should be modified to be asymmetric. The followings are some possible asymmetric designs of the stator and rotor.

- Non-uniform winding
- Non-uniform teeth shapes
- Non-uniform magnetization of permanent magnets
- Additional structure for reluctance modulation
- Additional coil in the rotor

If the asymmetric designs of the stator and rotor are combined, the motor can have different inductance profiles

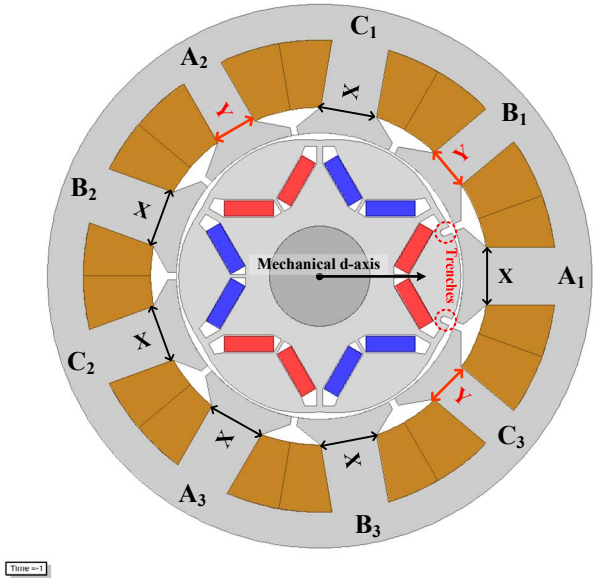

Figure 3. Motor design with rotor trenches and non-uniform teeth.

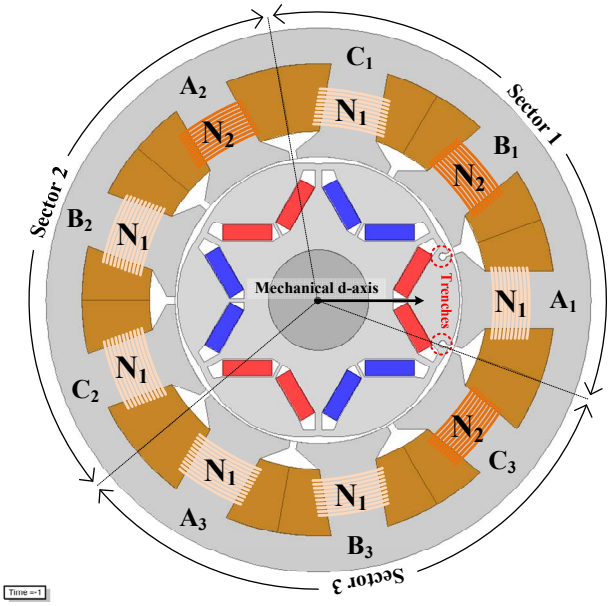

Figure 4. Proposed motor design.

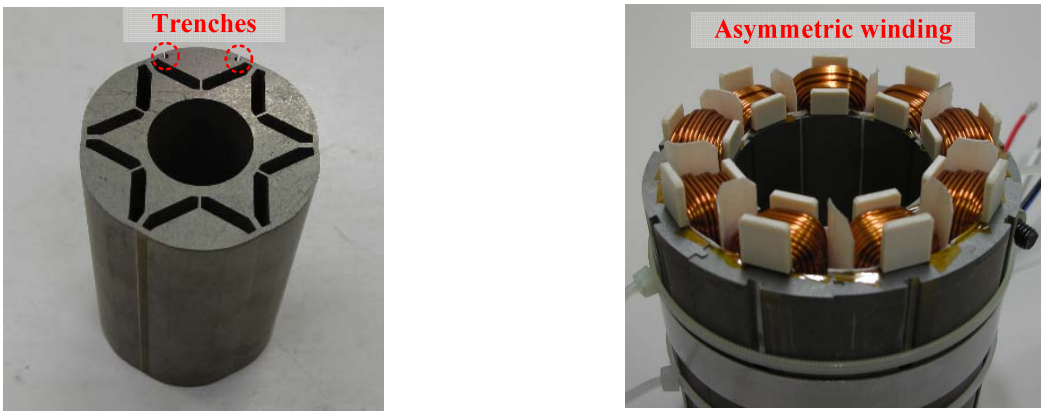

(a) Rotor with trenches

(b) Stator with asymmetric winding

Figure 5. Construction of prototype motor.

at every θ_{rm}. That is, θ_{rm} can be estimated by proper signal injection and processing.

As an example, the motor design in Fig. 2 can be considered as a possible design where additional shorted coil is buried on a specific spot of the rotor. And stator coil turn numbers N_1 and N_2 are non-uniformly distributed around the stator. Different from the rotor design in [4] where coils are installed at all magnetic poles, only a single coil is installed at a positive magnetic pole in Fig. 2. As a reference axis of the mechanical rotor position, Mechanical d-axis is defined in Fig. 2. Mechanical d-axis synchronously rotates with the coiled magnetic pole of the rotor. Since the rotor coil is magnetically coupled with stator coils, it forms secondary series L/R circuit in d-axis equivalent circuit of the motor whose parameters are expressed as $1/n^2$ times of its resistance and leakage inductance, where n indicates the turn ratio between the rotor coil and coupled stator coil. And n is determined by θ_{rm}. For example, the rotor coil is coupled with N_1 turn coil at θ_{rm}=0° and N_2 turn coil at θ_{rm}=40°. Since d-axis equivalent parameters vary according to θ_{rm}, θ_{rm} can be estimated by d-axis parameter measurement through signal injection.

Fig. 3 is another design. In the design, two trenches are dug at a specific positive magnetic pole and teeth widths are modulated. The rotor trenches make high reluctance part in the equivalent magnetic circuit. And the narrowed teeth are for utilizing saturation of the core. Applying positive d-axis current, the narrowed teeth are more saturated than other teeth, which results in higher reluctances of narrowed tooth. Then d-axis inductance, L_{ds}, varies according to the coupling of high reluctance rotor trench and high reluctance stator tooth. θ_{rm} can be estimated by the measurement of L_{ds} through signal injection.

Although the two designs in Fig. 2 and Fig. 3 work for the mechanical rotor position detection, they were not

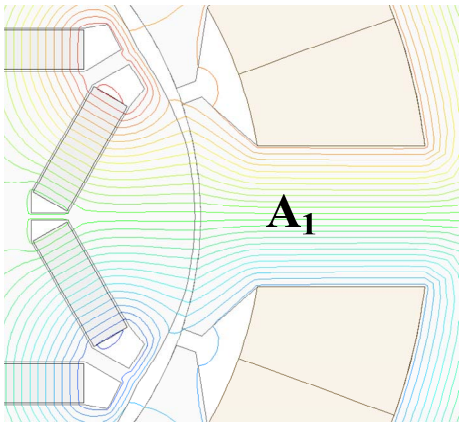

(a) Template motor design

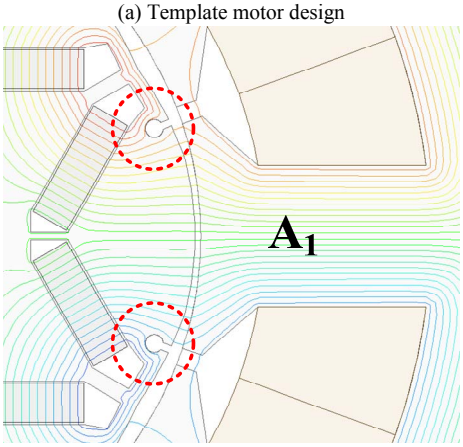

(b) Proposed motor design

Figure 6. Flux distributions near trenches.

selected for several reasons. In case of the design in Fig. 2, the rotor design is not good from the point of view of manufacturing since it requires coil insertion process. And the rotor coil brings about secondary dynamics in d-axis voltage and current relation that degrades dynamic performance of current control. Additional care should also be taken for overcurrent protection of the rotor coil. In case of the design in Fig. 3, the non-uniform teeth are not good for manufacturing. And the saturation of the narrowed teeth can also affect normal operation under heavy load condition.

B. Proposed Motor Design

Fig. 4 shows the proposed motor design. In this design, non-uniform winding and rotor trenches are applied. In the figure, coil turn N_1 is 30 and N_2 is 60. And the dimensions of the trenches are more optimized from that in Fig. 3. This design is actually constructed as a prototype as shown in Fig. 5.

For the explanation of how the proposed design works, the variation of inductance coming from the asymmetric motor structure should be investigated. Because coils of each phase are connected in series, the self-inductance of A-phase winding, L_A, can be given by (1), where L_{A1}, L_{A2}, and L_{A3} indicate the self-inductances of coils of A-phase wound in different slots.

$$L_A = L_{A1} + L_{A2} + L_{A3} \tag{1}$$

$$L_{A1} = \frac{N_{A1}^2}{\mathcal{R}_{A1}},\ L_{A2} = \frac{N_{A2}^2}{\mathcal{R}_{A2}},\ L_{A3} = \frac{N_{A3}^2}{\mathcal{R}_{A3}} \tag{2}$$

As expressed as (2), each self-inductance can be expressed by its equivalent reluctance and turn number, denoted as $\mathcal{R}$ and N. In the case of the template motor, due to its symmetric structure, A-phase inductance can be simply expressed as (3), where $\mathcal{R}_N$ means a nominal value of the reluctance.

$$L_A = 3\frac{N^2}{\mathcal{R}_N} = \frac{4800}{\mathcal{R}_N} \tag{3}$$

In case of the proposed motor design, Eq. (3) does not hold. Fig. 6 shows flux distributions of the template and modified motors when the mechanical d-axis is at mechanical 0°. Comparing Fig. 6(a) and (b), there is slight difference of flux lines near the trenches since the trenches form high reluctance parts. In this case, $\mathcal{R}_{A1}$ is larger than $\mathcal{R}_{A2}$ and $\mathcal{R}_{A3}$ as expressed in (4), where k is a constant which is lower than unity.

$$\mathcal{R}_{A1} = \mathcal{R}_N / k,\ \mathcal{R}_{A2} \approx \mathcal{R}_N,\ \mathcal{R}_{A3} \approx \mathcal{R}_N \tag{4}$$

$$L_{A1} = \frac{N_1^2}{\mathcal{R}_N / k},\ L_{A2} = \frac{N_2^2}{\mathcal{R}_N},\ L_{A3} = \frac{N_1^2}{\mathcal{R}_N} \tag{5}$$

Both $\mathcal{R}_{A2}$ and $\mathcal{R}_{A3}$ are assumed to be $\mathcal{R}_N$ since the rotor trenches would have negligible impact on A_2 and A_3 when θ_{rm}=0°. Then A-phase inductance when θ_{rm}=0° can be deduced as (6).

$$L_A = L_{A1} + L_{A2} + L_{A3} = \frac{N_1^2 + N_2^2 + kN_1^2}{\mathcal{R}_N} = \frac{4500 + 900k}{\mathcal{R}_N} \tag{6}$$

When θ_{rm}=40°, where the mechanical d-axis is aligned to B-phase, the inductance of B-phase can be derived as (7)-(8).

$$L_{B1} = \frac{N_2^2}{\mathcal{R}_N / k},\ L_{B2} = \frac{N_1^2}{\mathcal{R}_N},\ L_{B3} = \frac{N_1^2}{\mathcal{R}_N} \tag{7}$$

$$L_B = L_{B1} + L_{B2} + L_{B3} = \frac{2 \cdot N_1^2 + kN_2^2}{\mathcal{R}_N} = \frac{1800 + 3600k}{\mathcal{R}_N} \tag{8}$$

When θ_{rm}=80°, where the mechanical d-axis is aligned to C-phase, the inductance of C-phase can be derived as (9)-(10).

$$L_{C1} = \frac{N_1^2}{\mathcal{R}_N / k},\ L_{C2} = \frac{N_1^2}{\mathcal{R}_N},\ L_{C3} = \frac{N_2^2}{\mathcal{R}_N} \tag{9}$$

$$L_C = L_{C1} + L_{C2} + L_{C3} = \frac{N_1^2 + N_2^2 + kN_1^2}{\mathcal{R}_N} = \frac{4500 + 900k}{\mathcal{R}_N} \tag{10}$$

In the derivation of the self-inductances above, it is assumed that the rotor is aligned to the corresponding phases. And, self-inductances of phases in (5), (8), and (10) contribute to the rotor synchronous d-axis inductance, L_{ds}. This means

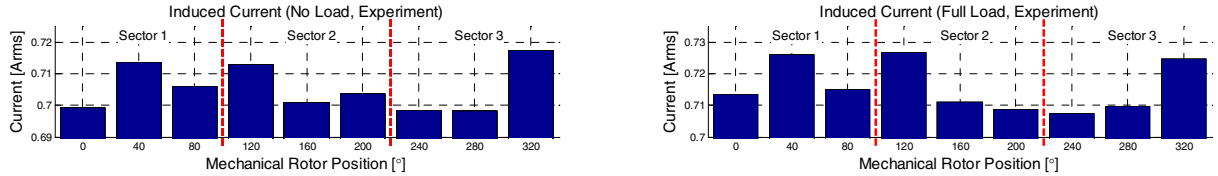

Figure 7. Induced current profiles.

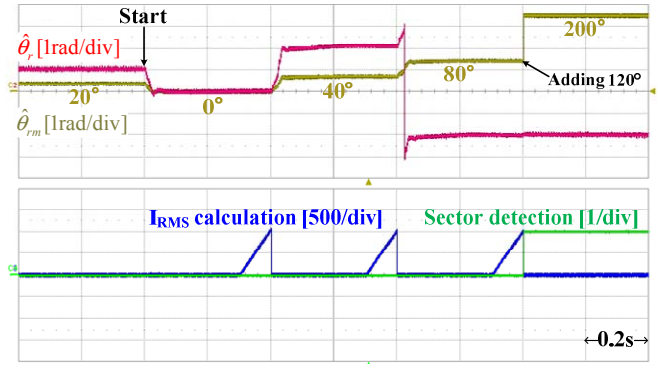

Figure 8. Mechanical sector detection of prototype motor.

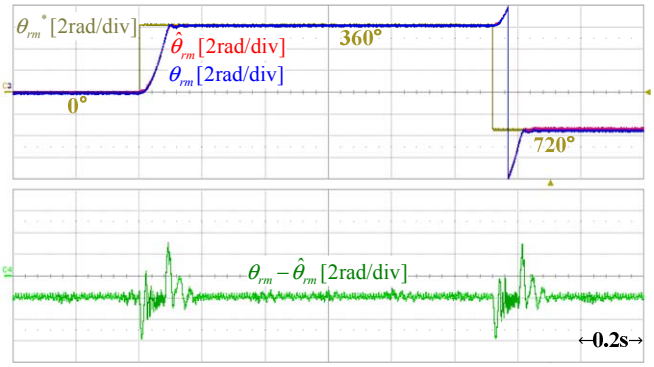

Figure 9. Mechanical position control of prototype motor.

that L_{ds} is modulated according to θ_{rm}. In detail, if the mechanical d-axis is aligned to higher-turn coil, L_{ds} becomes smaller. Injecting high frequency voltage to d-axis, L_{ds} can be reflected to the induced d-axis current. Fig. 7 shows experimentally measured current profile by injecting 140V 5kHz square wave voltage. Because the trenches at mechanical d-axis should be aligned to a stator coil, there are 9 possible alignment positions. As expected, induced current is larger when the rotor is aligned to higher number of turn coil. In the figure, each 360 degree of electrical angle has been noted as a sector. And, sector 1 corresponds to the first 360 degree of the rotation in electrical angle, which is equivalent to 0~120 degree in mechanical angle.

III. MECHANICAL ROTOR POSITION DETECTION ALGORITHM

The mechanical rotor position dependency of L_{ds} can be exploited for detecting the mechanical rotor position. From the tendency of the induced current profile in Fig. 7, mechanical 360° can be divided by 3 sectors as denoted in Fig. 4. In each sector, the largest current occurs at different phases. Because θ_r is already known by basic sensorless control described in [3], θ_{rm} can be calculated by sector identification. The step-by-step procedure for the mechanical rotor position detection can be summarized as follows:

- Step 1: Run the basic sensorless algorithm based on high frequency signal injection [3] to detect initial value of θ_r.
- Step 2: Under sensorless position control mode, align the rotor position to nearest A-, B-, and C-phases and calculate the RMS value of d-axis current ripple at each phase. During the alignment sequence, the mechanical d-axis does not cross between sectors. Initial rotor stroke angle in the alignment sequence is mechanical 100° in the worst case when initial value of θ_{rm} is exactly between any two sectors.
- Step 3: Compare the induced currents with the profile in Fig. 7. If the largest current is at A-phase, the sector is 2. If the largest current is at B-phase, the sector is 1. And if the largest current is at C-phase, the sector is 3. Because relative comparison of the measured current is used, this algorithm would be robust to current sensing error. Based on the already identified $\hat{\theta}_r$ and sector number, $\hat{\theta}_{rm}$ can be easily calculated as (11).

$$\hat{\theta}_{rm} = \hat{\theta}_r / 3 + \Delta_{Sector} \cdot \frac{2}{3}\pi \tag{11}$$

In (11), Δ_{Sector} indicates the difference of sector numbers from initial guess and from the identification.

Fig. 8 shows experimental waveforms of the mechanical rotor position detection. Under full load condition, θ_{rm} is initially 140° in sector 2. Since there is no information of θ_{rm} in the initial start-up procedure, $\hat{\theta}_{rm}$ is assumed to be simply one third of $\hat{\theta}_r$, 20°. When the mechanical rotor position detection algorithm starts, the rotor is aligned to A-, B-, and C-phases in sequence. At each alignment, RMS value of d-axis current is calculated for 100ms. After the 3 alignments, mechanical sector is identified by comparing RMS values at each alignment position. Finally, $\hat{\theta}_{rm}$ is corrected by adding 120°. Even after the correction, $\hat{\theta}_r$ is not changed because it is bounded between -180° and 180°.

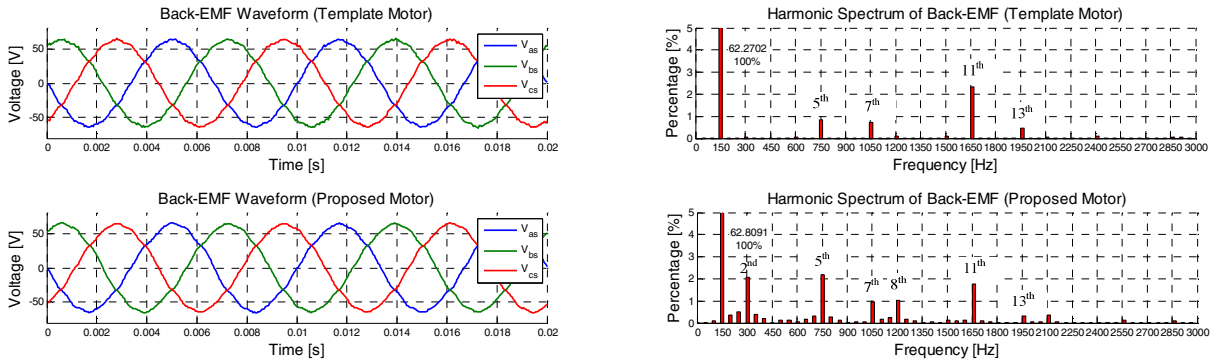

(1) Back-EMF waveforms (b) Harmonic spectrums

Figure 10. Back-EMF characteristic (no load, 3000r/min).

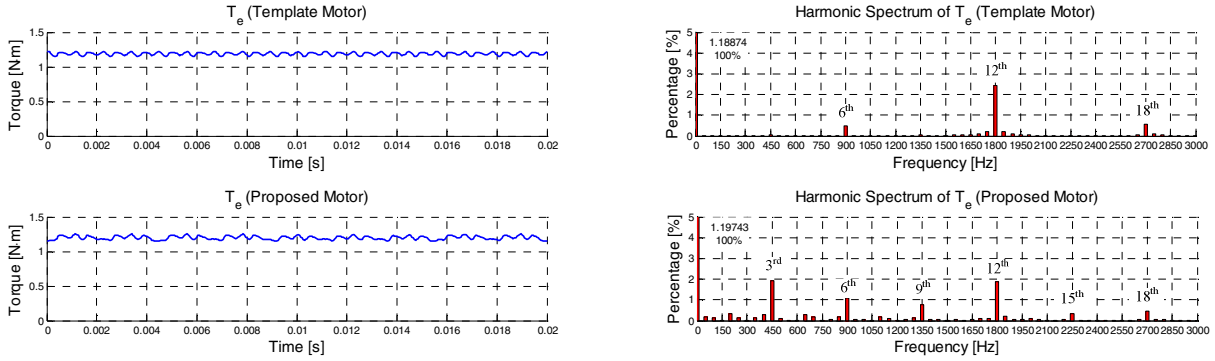

(1) Torque waveforms (b) Harmonic spectrums

Figure 11. Torque characteristic (full load, 3000r/min).

The detection algorithm also works for initial mechanical rotor positions other than 140°.

After the detection of the mechanical rotor position, actual rotor position can be controlled. Fig. 9 shows experimental waveforms of the absolute positioning of the rotor, where θ_{rm}^{*} means position reference. Under full load condition, θ_{rm}^{*} is initially 0° and jumped up to 360° and 720° in sequence. Even under the step change of θ_{rm}^{*}, the rotor position well tracks its command. The steady state error of position estimation comes from the saturation of core by current [5]-[6], not from the sensorless control itself. In the steady state, the error is about 3° in mechanical angle.

IV. BASIC CHARACTERISTICS

Due to the asymmetric structure of the proposed motor design, there is inevitable degradation of basic characteristics. Fig. 10 and 11 show back-EMF and torque characteristics from FEM simulations. As shown in Fig. 10 and 11, back-EMF and torque from the prototype motor contains additional low order harmonic components. These harmonic components come from the rotor trenches. If the size of the trenches is getting smaller, the low order harmonics could be smaller. But, the current profile for the mechanical rotor position detection in Fig. 7 becomes vague. Hence, the trench size in Fig. 6 has been determined from the trade-off consideration between back-EMF and torque characteristics and the mechanical rotor position detection capability.

There is also unbalanced magnetic pull (UMP) in the proposed motor coming from its asymmetric structure. UMP is radial directional force which does not contribute to the torque. Since UMP can cause significant vibration and acoustic noise problem in the motor drive system, UMP should be considered in the motor design. Fig. 12 shows the UMP of the proposed motor design under rated condition computed by FEM simulator. UMP is calculated by Maxwell's stress tensor from magnetic flux density at the mid-airgap between the rotor and stator [7]-[8]. From the results of the calculation of UMP, it is known that 47.7N force in average is applied to the axis of the rotor. Differerent from other asymmetric winding machines, UMP does not rotate around the axis, but strokes between -35° and 128°. Because higher-turn coils at the right-top side make more pulling force, the direction of UMP is also biased to the right-top direction.

The non-uniformity of stator winding is designed based on the trade-off consideration between UMP and the mechanical rotor position detection capability. With larger difference of N_1 and N_2, the current profile in Fig. 7 becomes clearer. However, UMP would be getting severe

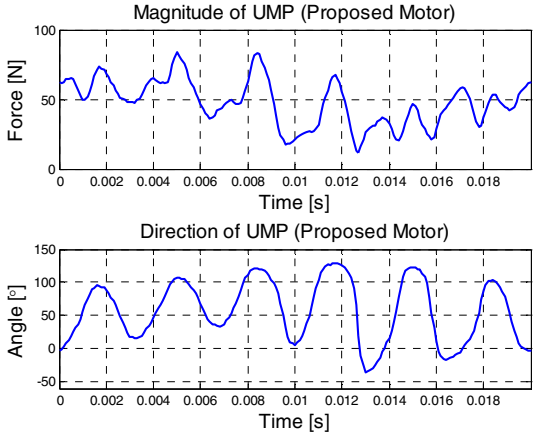

Figure 12. Unbalanced magnetic pull (full load, 3000r/min).

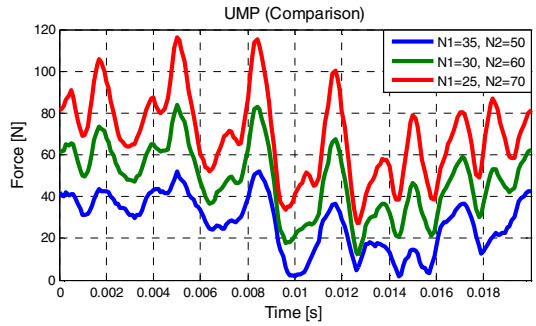

Figure 13. Unbalanced magnetic pull with various N_1 and N_2 combinations (full load, 3000r/min).

with larger difference of N_1 and N_2. Fig. 13 shows UMPs from various N_1 and N_2 combinations. With N_1=25 and N_2=70 combination, UMP is more severe in Fig. 13. But with N_1=35 and N_2=50, the current profile in Fig. 7 becomes too unclear to distinguish the difference of current magnitudes. N_1=30 and N_2=60 is selected from the consideration of the trade-off relation.

V. CONCLUSIONS

In this paper, a modified design and control strategy of sensorless drive of IPMSM for mechanical rotor position control capability has been proposed. Contrary to the conventional design concept, the proposed IPMSM has asymmetric structure: Asymmetric stator winding and asymmetric rotor shape. By the interaction of rotor and stator asymmetries, d-axis inductance is modulated according to the mechanical rotor position. In conjunction with the proposed control strategy, the mechanical rotor position without absolute encoder/resolver can be identified and controlled within 3˚ mechanical degree accuracy under full load condition. Due to the intentional asymmetries, the degradation of basic performance such as torque ripple is inevitable but the ripple is in allowable range, less than 2%.

REFERENCES

[1] S. Morimoto, K. Kawamoto, M. Sanada, and Y. Takeda, "Sensorless control strategy for salient-pole PMSM based on extended EMF in rotating reference frame," *IEEE Trans. Ind. Appl.*, vol. 38, no. 4, pp. 1054-1061, Jul./Aug. 2002.

[2] J. I. Ha, and S. K. Sul, "Sensorless field-orientation control of an induction machine by high-frequency signal injection," *IEEE Trans. Ind. Appl.*, vol. 35, no. 1, pp. 45-51, Jan./Feb. 1999.

[3] Y. D. Yoon, S. K. Sul, S. Morimoto, and K. Ide, "High bandwidth sensorless algorithm for AC machines based on square-wave-type voltage injection," *IEEE Trans. Ind. Appl.*, vol. 47, no. 3, pp. 1361-1370, May/Jun. 2011.

[4] A. Faggion, N. Bianchi, and S. Bolognani, "Ringed-pole permanent-magnet synchronous motor for position sensorless drives," *IEEE Trans. Ind. Appl.*, vol. 47, no. 4, pp. 1759-1766, Jul./Aug. 2011.

[5] N. Bianchi and S. Bolognani, "Influence of rotor geometry of an IPM motor on sensorless control feasibility," *IEEE Trans. Ind. Appl.*, vol. 43, no. 1, pp. 87-96, Jan./Feb. 2007.

[6] Y. Li et al. "Improved Rotor-Position Estimation by Signal Injection in brushless AC motors, accounting for cross-coupling magnetic saturation," *IEEE Trans. Ind. Appl.*, vol. 45, no. 5, pp. 1843-1850, Sept../Oct.. 2009.

[7] G. Jang et al. "Torque and unbalanced magnetic force in a rotational unsymmetric brushless DC motors," *IEEE Trans. Ind. Magn.*, vol. 32, no. 5, pp. 5157-5159, Sept 1996.

[8] Z. Zhu, M. Jamil, and L. Wu "Influence of lot and pole number combinations on unbalanced magnetic force in PM machines with diametrically asymmetric windings," *IEEE Trans. Ind. Appl.*, vol. 49, no. 1, pp. 19-30, Jan./Feb. 2013.